

# Quantum Feature Space of Qubit in Arbitrary Bath

Chris Wise<sup>1,\*</sup>, Akram Youssry<sup>2</sup>, Alberto Peruzzo<sup>2,3</sup>, Jo Plested<sup>1</sup>, and Matt Woolley<sup>4</sup>

<sup>1</sup>School of Systems and Computing, University of New South Wales, Canberra, ACT, 2601, Australia

<sup>2</sup>Quantum Photonics Laboratory and Centre for Quantum Computation and Communication Technology, RMIT University, Melbourne, VIC 3000, Australia

<sup>3</sup>Qubit Pharmaceuticals, Advanced Research Department, Paris, France

<sup>4</sup>Centre for Engineered Quantum Systems, University of New South Wales, Canberra, ACT, 2601, Australia

\*Author to whom any correspondence should be addressed.

E-mail: [c.wise@unswalumni.com](mailto:c.wise@unswalumni.com)

August 2024

**Abstract.** Quantum computers offer the potential to solve otherwise intractable computational problems. However, they remain in a relatively early stage of development. Further progress depends upon an enhanced ability to enact high-fidelity qubit control in the presence of noise due to a coupled bath. The development of qubit control protocols has traditionally leveraged a characterisation of the bath coupling via its power spectral density.

Youssry et al. [1] introduced an alternative, so-called noise operator formalism. This approach allows one to characterise the influence of an arbitrary bath on the evolution of a qubit in the presence of a given set of control pulses. Previously, these noise operators were inferred using a neural network-based approach based. Here, we show that the noise operators may be directly, accurately, and efficiently inferred using a regression-based approach. The training data is obtained from simulations based on the work of Perrier et al. [2] that generated *QDataSet*.

The noise operator description admits an efficient parameterisation; we refer to this parametrisation as the *quantum feature space* of the qubit dynamics resulting from noise arising from arbitrary coupled bath. We show that the Euclidean distance defined over the quantum feature space provides an effective method for classifying noise processes in the presence of a given set of controls. We demonstrate a decision tree's effectiveness in classifying the stationarity and broad class of noise processes perturbing a qubit, with the input being the quantum feature space.

The quantum feature space characterisation of a qubit in the presence of an arbitrary bath provides a valuable tool for its characterisation and control. It offers a tool that could be generalised to multi-qubit systems.

*Keywords:* quantum control, quantum features, classification, clustering

## 1. Introduction

Quantum computers offer the potential to solve otherwise intractable computational problems. However, quantum computers have yet to perform commercially valuable computations as the technology remains in the so-called noisy intermediate-scale quantum (NISQ) era [3]. Intermediate here refers to quantum computers with 50 to a few hundred qubits, and the noise primarily refers to the imperfect control of qubits. To move beyond NISQ, we must account for and mitigate this noise [3].

Noise in quantum computers resulting in qubits losing coherence (decoherence) is due to unwanted bath coupling [4]. One way to mitigate decoherence is to decouple the qubit from the bath by applying a control field, a technique which is known as dynamical decoupling and is implemented as a series of pulses [5].

Predicting qubit evolution given an arbitrary bath and control pulse sequences is non-trivial [1, 6]. The problem can be simplified if assumptions are made about the bath (e.g., the bath is characterised by stationary zero-mean Gaussian noise) [7, 8]. However, making minimal assumptions about the bath is desirable to increase the applicability of developed control methods.

Previous work has used machine learning (ML) techniques for qubit noise spectroscopy and control [7, 9, 8, 10, 11, 1, 6]. However, the features used to train these algorithms were classical (i.e. observable expectations), and no exploration of their mapping to quantum operators was explored. We introduce in this paper *quantum feature spaces* and show that no expensive algorithms are needed to classify the noise affecting a qubit. Instead, we use the Euclidean distance within the quantum feature space for classification.

Sec. 2 provides an overview of analytical and ML approaches to qubit control and noise spectroscopy of baths. Sec. 3 reviews the noise operator formalism introduced in [1, 6], which separates closed-system and open-system dynamics. We show in Sec. 4 how these noise operators can be deduced from observable expectations, forming our quantum feature spaces. Sec. 5 demonstrates the utility of the quantum feature space where we use the Euclidean distance to identify an unknown noise process affecting a qubit and a decision tree to classify noise processes. This section also studies how control and noise parameters map to the quantum feature space. Future work is discussed in Sec. 6. Fig. 1 illustrates how the quantum feature space is generated and then used for downstream tasks such as classification and clustering.

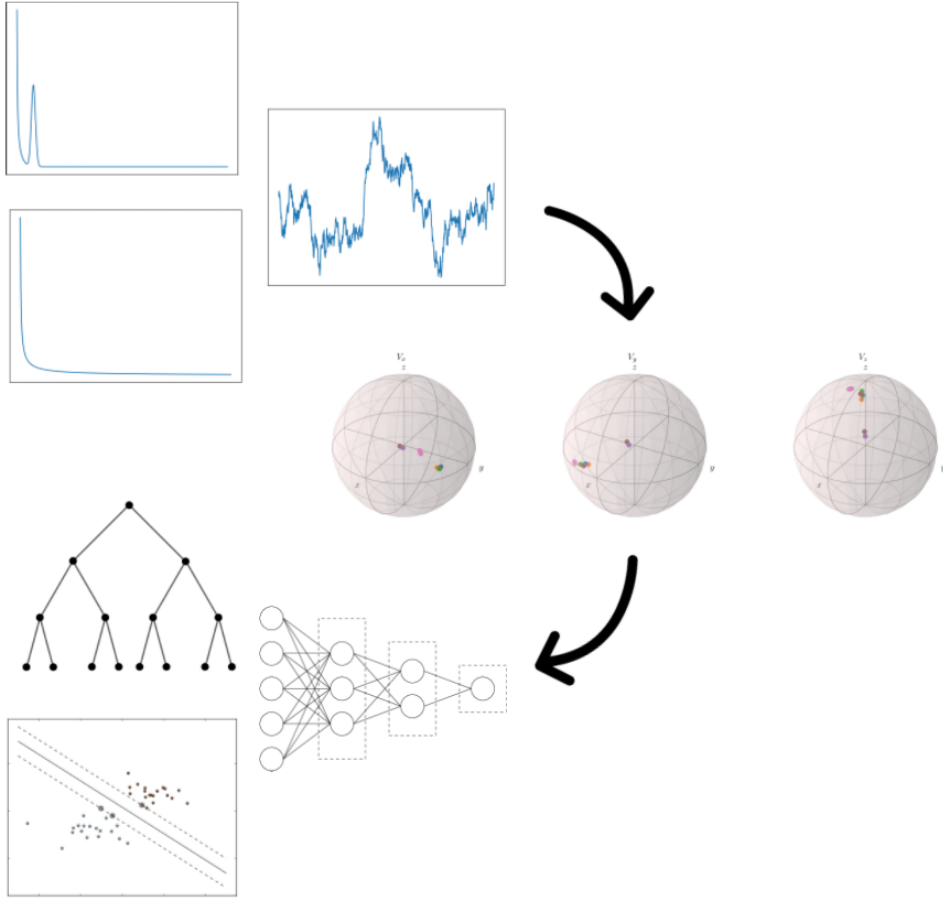


**Figure 1.** Schematic of the quantum feature space. Various noise processes generate data points in the quantum feature space. This quantum feature space can then be used for downstream tasks such as classification and clustering using decision trees, k-means, and neural nets.

## 2. Previous Work

### 2.1. Dynamical Decoupling and Noise Spectroscopy

Control pulses to decouple quantum systems from baths was first studied in nuclear magnetic resonance imaging [12, 13]. Control pulses to address decoherence is known as dynamical decoupling. Within this framework, control pulses are applied for a time  $\tau$  and then turned off for time  $\tau$ , and this pattern is repeated  $N$  times. This oscillating pulse sequence design is the Carr-Purcell-Meiboom-Gill (CPMG) sequence [14, 15].

Álvarez and Suter (AS) proposed a modified CPMG sequence to perform qubit spectroscopy [16]. AS pulses are part of a family of pulses used for so-called dynamical decoupling noise spectroscopy. AS pulses measure qubit coherence as a function of time via,

$$C(t) = \frac{\langle \rho_{01}(t) \rangle}{\langle \rho_{01}(0) \rangle} \quad (1)$$

where  $\rho_{01}(t) = \langle 0|\rho(t)|1\rangle$ ,  $\langle \cdot \rangle$  denotes ensemble averaging over many repeated experiments, and  $\langle 0|\rho(0)|1\rangle \neq 0$  [8].

These coherence curves are fitted to coherence curves corresponding to parametric noise spectra [17, 18]. However, this method requires an accurate model of system dynamics [7], which can be challenging to develop in general [19]. Further, if an inappropriate parametric noise spectrum is chosen *a priori*, the estimated noise spectrum is an inappropriate model of system dynamics and subsequently, control pulses optimised using this system model will likely be ineffective [19].

More direct methods of noise spectroscopy include techniques like two-point correlation (TPC), which measures the correlation function of the noise by implementing gates at different times and measuring the change in the qubit state [20]. The Fourier transform of this correlation function gives the noise spectrum. However, this method can be resource-intensive, time-consuming, computationally expensive and requires the noise to be stationary [17, 7, 9, 8].

The authors of [8] developed a quantum noise spectroscopy (QNS) method that used the Fourier transform of free induction decay measurements of coherence curves. The method accurately recovered the correct noise spectra and outperformed previous decoupling schemes while significantly reducing experimental overhead. However, the method makes several assumptions that limit the work's applicability. For example, the authors assume only qubit dephasing, where the qubit thermal relaxation process occurs over a much longer time scale than phase randomisation, and that the frequency fluctuations of a qubit are subject to stationary zero-mean Gaussian noise.

## 2.2. Machine Learning for Qubit Noise Spectroscopy and Control

In [7], researchers used deep learning techniques to infer accurate qubit noise spectra. The technique used coherence curves as input to a recurrent neural network with a feedforward neural network head to estimate the noise spectrum. They showed that the model could accurately estimate the qubit noise spectrum using only the coherence curves and outperformed the standard noise spectroscopy techniques.

Researchers in [9] further demonstrated the effectiveness of deep learning by using it to reconstruct the power spectral density of an ensemble of carbon impurities around a diamond's nitrogen-vacancy centre. The study's findings underscore the increased accuracy of deep learning models over standard noise spectroscopy techniques.

Despite the success of [7, 9], both approaches are limited by their use of deep learning models, specifically the expense of training deep learning models and the need for large datasets. This expense is an issue as noise processes in quantum systems can drift over time [21, 22], necessitating new training data and model retraining potentially daily or even hourly. Additionally, noise profiles may change from one physical qubit to another [23], so a specific model may be required for each qubit, which does not scale

well. This variability of qubit noise profiles motivates the need to move beyond deep learning models for noise spectroscopy and to find feature spaces that can be used to classify qubit noise profiles without deep learning models.

Mavadia et al.[10] used techniques from control theory and ML to predict a qubit's evolution, and these predictions were used to suppress decoherence in the case of limited measurements. They implemented a time-division multiplexed approach and employed predictive feedback during sequential but time-delayed measurements to reduce the Dicke effect. Specifically, they utilised a supervised learning algorithm that predicted future qubit states based on past measurement outcomes, optimising weighting coefficients for prediction accuracy.

Gupta and Biercuk [11] compared various ML algorithms for state estimation and prediction of qubit's evolution subject to classical, non-Markovian dephasing noise. They investigated the performance of Kalman Filters and Gaussian Process Regression algorithms. The study demonstrated the superior performance of the Kalman Filter over Fourier-based approaches, focusing on filter optimisation for enhanced prediction. The authors also explored several Gaussian Process Regression realisations with different kernels, concluding that these were generally unsuitable for forward prediction.

Youssry et al. [1] introduced a grey-box model separating control and system-bath dynamics. Time-dependent Hamiltonians and unitaries specified the control dynamics, and a form of recurrent neural network (a gated recurrent unit) was used to predict the system-bath dynamics associated with control pulses.

The input to this GRU was a sequence of vectors; parameterised control pulses. The model output was the parameterisation of a noise operator. The authors showed that the grey-box model could be used for qubit control pulse optimisation and qubit noise spectroscopy. The formalism used in this work is discussed in greater detail in Sec. 3.

The grey-box model approach was subsequently used for qubit control optimisation in the presence of a non-Markovian bath [6].

Within the current literature, the input to ML and deep learning algorithms have all been related to expectation values and/or characteristics of control pulses. However, we show that richer feature spaces could be found using parameters more directly related to the bath (here, it is the operator representation of bath influence on system dynamics), allowing for noise classification without needing expensive deep-learning models. Thus, as noise drifts over time or is different between physical qubits, there is no need for expensive model retraining. Larger, more expensive models were needed in the previous work as the model had to learn to map expectations and other such inputs to an internal representation of the bath and then map this internal representation to the characteristics of the bath. However, we demonstrate that with parameters directly related to bath dynamics, a simple model can be used to classify the noise, as the model does not need to learn to map from expectations to a representation of the bath.

With this, we developed a method to deduce the parameters of an operator that encodes the bath's influence on system dynamics while making minimal assumptions about the bath such that it could be used beyond toy problems and have utility for a broad range of physically realised qubits.

### 3. Noise Operator Formalism

#### 3.1. Separating Control Dynamics From System-Bath Interaction Dynamics

The Hamiltonian describing a controlled qubit (the system) interacting with a bath is,

$$H(t) = H_{\text{ctrl}}(t) + H_{\text{SB}}(t) \quad (2)$$

where the control Hamiltonian is,

$$H_{\text{ctrl}}(t) = \Omega \frac{\sigma_z}{2} + \sum_{j=\{x,y,z\}} f_j(t) \frac{\sigma_j}{2} \quad (3)$$

where  $\Omega$  is the qubit's energy gap and  $f_j(t)$  is a control pulse along the given axis, and the system-bath Hamiltonian is,

$$H_{\text{SB}}(t) = \sum_{j=x,y,z} \sigma_j \otimes B_j(t) \quad (4)$$

with  $B_j(t) = \hat{B}_j(t) + \beta_j(t)I_B$  capturing a quantum bath via the operator  $\hat{B}_j(t)$  and classical noise via the stochastic process  $\beta_j(t)$ .

We are interested in the expected value of a system (qubit) observable  $O$  at time  $T$  given an initial system (qubit) state  $\rho$ , where  $T$  represents the total time of the control pulse sequence. This is given by,

$$\mathbb{E}\{O(T)\}_{\rho} = \langle \text{Tr} [U(T) (\rho \otimes \rho_B) U(T)^\dagger O] \rangle \quad (5)$$

where  $U(T) = \mathcal{T}e^{-i \int_0^T H(s) ds}$  is the time-ordered exponential of the time-dependent Hamiltonian in Eq. (2),  $\langle \cdot \rangle$  denotes classical averaging over the random processes  $\beta_j(t)$ , and  $\rho_B$  is the initial state of the bath.

We then decompose the total system-bath evolution into a product of system-bath dynamics and control dynamics. To do this, Youssry et al. [1] introduced a so-called *toggling frame*, defined by the time-ordered control unitary,

$$U_{\text{ctrl}}(t) = \mathcal{T}e^{-i \int_0^t H_{\text{ctrl}}(s) ds} \quad (6)$$

Then, the system-bath Hamiltonian in the toggling frame is,

$$H_{\text{SB}}^{\text{tog}}(t) = U_{\text{ctrl}}^\dagger(t) H_{\text{SB}}(t) U_{\text{ctrl}}(t) \quad (7)$$

with the associated unitary,

$$U_{\text{SB}}^{\text{tog}}(t) = \mathcal{T}e^{-i \int_0^t H_{\text{SB}}^{\text{tog}}(s) ds} \quad (8)$$

It can be shown that,

$$U_{\text{SB}}(t) = U_{\text{ctrl}}(t)U_{\text{SB}}^{\text{tot}}(t)U_{\text{ctrl}}^\dagger(t) \quad (9)$$

which allows us to rewrite Eq. (5) as,

$$\mathbb{E}\{O(T)\}_\rho = \text{Tr} [V_O(T)U_{\text{ctrl}}(T)\rho U_{\text{ctrl}}^\dagger(T)O] \quad (10)$$

where

$$V_O(T) = \left\langle O^{-1}U_{\text{SB}}^\dagger(T)OU_{\text{SB}}(T) \right\rangle_B \quad (11)$$

with  $\langle \cdot \rangle_B = \langle \text{Tr}_B[\cdot \rho_B] \rangle$  representing classical averaging over the partial trace taken with respect to the bath. Physically, we interpret  $V_O$  as a so-called *noise operator* that encodes the influence of the system-bath interaction on the qubit dynamics.

### 3.2. Decomposition of the System-Bath Operator

When our system-bath Hamiltonian consists of only classical noise processes, one can move  $O^{-1}$  in Eq. (11), and write,

$$V_O = O^{-1} \left\langle U_{\text{SB}}^\dagger OU_{\text{SB}} \right\rangle \quad (12)$$

where time argument  $T$  has been omitted for brevity. Before continuing, it is important to note some of the mathematical properties of the  $V_O$  operator as they subsequently inform restrictions on its parameterisation. Specifically,  $\left\langle U_{\text{SB}}^\dagger OU_{\text{SB}} \right\rangle$  is trace bounded by one, is Hermitian, and has real eigenvalues between  $-1$  and  $1$  [1].

One could parameterise  $V_O$  as a general complex matrix. However, a given prediction of a complex matrix by a trained model would likely not satisfy the above properties. Further, it requires  $2n^2$  (where  $n$  is the matrix dimension) free parameters to be predicted. Thus, one is motivated to find a more efficient parameterisation of  $V_O$ .

One such efficient parameterisation of  $V_O$  is provided by its eigendecomposition. This eigendecomposition contains a diagonal matrix  $D_O$  whose entries are real numbers in the interval  $[-1, 1]$  and whose sum also lies in the interval  $[-1, 1]$ , and a general unitary matrix  $Q$ . Thus Eq. (12) can be rewritten as

$$V_O = O^{-1}Q_O D_O Q_O^\dagger \quad (13)$$

In the case of a qubit, we start with a factorisation of a general  $2 \times 2$  unitary operator,

$$Q_O = \begin{bmatrix} e^{i\psi_O} & 0 \\ 0 & e^{-i\psi_O} \end{bmatrix} \begin{bmatrix} \cos \theta_O & \sin \theta_O \\ -\sin \theta_O & \cos \theta_O \end{bmatrix} \begin{bmatrix} e^{i\Delta_O} & 0 \\ 0 & e^{-i\Delta_O} \end{bmatrix}, \quad (14)$$

where  $\psi_O, \theta_O, \Delta_O \in \mathbb{R}$  and the diagonal matrix  $D_O$  of Eq. (13) is constructed as

$$D_O = \begin{bmatrix} \mu_O & 0 \\ 0 & -\mu_O \end{bmatrix} \quad (15)$$

where  $\mu_O \in [0, 1]$ . The matrix  $D_O$  can be generalised to non-unital channels [1], but this paper will focus on unital channels. An unital channel is a quantum channel that maps the identity operator to the identity operator, and a non-unital channel does not [24].

#### 4. Deducing Noise Operators from Observable Expectations

The previous grey-box approach to qubit control of [1, 6] used expectations and control pulse amplitudes to train a model, both classical feature spaces. This motivated us to develop a method to deduce the  $V_O$  operators and their parameters from observable expectations. This allowed us to understand the properties of the qubit bath over time. The  $V_O$  matrices are quantum operators, where it was hypothesised that the feature space formed from these operators' parameters is richer than those used in previous work.

Substituting Eq. (13) into Eq. (10) gives,

$$\mathbb{E}\{O(T)\}_\rho = \text{Tr} \left[ Q_O D_O Q_O^\dagger U_{\text{ctrl}} \rho U_{\text{ctrl}}^\dagger \right] \quad (16)$$

To calculate the mapping between expectations and  $V_O$  operators, one must understand *a priori* the generalised structure of  $Q_O D_O Q_O^\dagger$ . Recalling the definition of  $Q_O$ , we find  $Q_O D_O Q_O^\dagger$  is,

$$\begin{bmatrix} \mu_O \cos(2\theta_O) & -e^{2i\psi_O} \mu_O \sin(2\theta_O) \\ -e^{-2i\psi_O} \mu_O \sin(2\theta_O) & -\mu_O \cos(2\theta_O) \end{bmatrix} \equiv \begin{bmatrix} \gamma_O & \alpha_O + \beta_O i \\ \alpha_O - \beta_O i & -\gamma_O \end{bmatrix} \quad (17)$$

Now  $U_{\text{ctrl}} \rho U_{\text{ctrl}}^\dagger$  must be Hermitian, with trace one, such that,

$$U_{\text{ctrl}} \rho U_{\text{ctrl}}^\dagger = \begin{bmatrix} a_\rho & b_\rho + c_\rho i \\ b_\rho - c_\rho i & 1 - a_\rho \end{bmatrix} \quad (18)$$

with  $0 \leq a_\rho \leq 1$ .

We can now calculate the generalised form of  $\mathbb{E}\{O(T)\}_\rho$  in terms of the newly introduced parameters,

$$\mathbb{E}\{O(T)\}_\rho = 2b_\rho \alpha_O + 2c_\rho \beta_O + (2a_\rho - 1)\gamma_O \quad (19)$$

For each observable, there are six initial states, so to find solutions  $\alpha_O, \beta_O, \gamma_O$  for each observable, we need to solve an over-determined system of six equations with three unknowns,

$$\begin{bmatrix} 2b_{\rho_{x+}} & 2c_{\rho_{x+}} & (2a_{\rho_{x+}} - 1) \\ 2b_{\rho_{x-}} & 2c_{\rho_{x-}} & (2a_{\rho_{x+}} - 1) \\ \vdots & \vdots & \vdots \\ 2b_{\rho_{z-}} & 2c_{\rho_{z-}} & (2a_{\rho_{z-}} - 1) \end{bmatrix} \begin{bmatrix} \alpha_O \\ \beta_O \\ \gamma_O \end{bmatrix} = \begin{bmatrix} \mathbb{E}\{O\}_{\rho_{x+}} \\ \mathbb{E}\{O\}_{\rho_{x-}} \\ \vdots \\ \mathbb{E}\{O\}_{\rho_{z-}} \end{bmatrix} \quad (20)$$

with  $\rho_{x+}, \rho_{x-}, \dots, \rho_{z-}$  being the standard eigenstates of the Pauli matrices.

The best-fit solution can be found using the Moore-Penrose inverse [25]. The Moore-Penrose inverse can be computed efficiently and parallelised across control pulses and expectation pairs using a GPU and libraries such as *Pytorch* [26] or *NumPy* [27]. Once the best-fit solution is found, the  $V_O$  operator can be constructed using Eq. (13).

Ground truth expectations and the corresponding  $V_O$  operators from *QDataSet* [2] were used to test the validity of this method. A batch of 1000  $V_O$  operators was estimated with no expensive neural networks, with the maximum and average error between matrix entries being 0.000008 and 0.000002, respectively.

Evaluating the eigenvalues of the parameterisation of  $Q_O D_O Q_O^\dagger$  in Eq. (17) yields

$$\mu_O = \sqrt{\gamma_O^2 + \alpha_O^2 + \beta_O^2} \quad (21)$$

where  $0 \leq \mu_O \leq 1$ . Equating the parameterised forms of  $Q_O D_O Q_O^\dagger$  we find,

$$\theta_O = \frac{1}{2} \arccos \left( \frac{\gamma_O}{\mu_O} \right) \quad (22)$$

$$\psi_O = \frac{1}{2} \text{Im} \left[ \ln \left( \frac{\alpha_O + \beta_O i}{\mu_O \sin(2\theta_O)} \right) \right] \quad (23)$$

where  $0 \leq \theta_O \leq \frac{\pi}{2}$ , and  $-\frac{\pi}{2} \leq \psi_O < \frac{\pi}{2}$ . To allow visualisation on the unit 2-sphere, we define  $\tilde{\theta}_O = 2\theta_O$  and  $\tilde{\psi}_O = 2\psi_O$ , giving  $0 \leq \tilde{\theta}_O \leq \pi$  and  $-\pi \leq \tilde{\psi}_O < \pi$ .

This section has shown that the  $V_O$  operator can be deduced from observable expectations, and then we can easily determine the parameters  $\mu_O$ ,  $\theta_O$ , and  $\psi_O$ , which form the quantum feature space.

## 5. Using the Quantum Feature Space

Using the quantum feature space, we may classify an unknown noise process, visualise the effects of changing control pulse width and noise strength, and optimise control pulses. To do this, we started with noise models and realisation generation methods following that of *QDataSet* [2]. All noise processes acted along the  $x$  and  $z$  axes, with the noise processes being correlated along the  $x$  and  $z$  axes. This correlation was achieved by setting the noise values along one axis to be the absolute value of the other axis values (similar to noise profile N6 in *QDataSet*).

The following noise processes were explored:

- a noise process with a  $1/f$  noise power spectral density (PSD) (N5 in *QDataSet*)
- a noise process with a  $1/f$  noise PSD with a Gaussian bump in the PSD (N1 in *QDataSet*)
- a Gaussian coloured noise process (N2 in *QDataSet*)

There were six different noise processes in total. The first three were the above noise processes acting along the  $x$  axis, with the correlated noise process acting along the  $z$  axis. The other three noise processes were similar, but the noise was made non-stationary by multiplying a deterministic time-domain signal with the stationary noise.

The second noise process ( $1/f$  with a bump) was chosen as it shared similarities with the first noise process ( $1/f$ ). It was hypothesised that these two noise processes would result in points close together in the quantum feature space. Conversely, the third (stationary coloured) was chosen as it was hypothesised that it would result in points far from the first two noise processes' points.

Control pulses were applied along the  $x$ -axis for all simulations, where the control pulses were approximations of CPMG pulses. To achieve CPMG pulses, we created Gaussian-shaped pulses of the form

$$f_j(t) = \sum_{n=1}^{n_{\max}} A_n e^{-\frac{(t-\tau_n)^2}{2\sigma^2}} \quad (24)$$

where  $\sigma = \frac{T}{\lambda M}$ ,  $\lambda \in \mathbb{R}^+$  is the pulse width,  $T$  is the total time,  $M$  is the number of time steps,  $\tau_n = \left(\frac{n-0.5}{n_{\max}}\right)T + \delta_\tau$ ,  $\delta_\tau \in \mathbb{R}$  and was used to add jitter to the pulse, and  $A_n$  is the amplitude of the  $n^{\text{th}}$  pulse.

For all experiments  $n_{\max} = 5$ , and 1024 discrete time steps were used. Additionally, ensemble averaging was performed over 2000 realisations of the noise process for a given control pulse sequence.

### 5.1. Black Box Classification of Bath Through Quantum Feature Space

We conducted a series of simulations to test the ability of the quantum feature space to classify distinct noise processes, where the quantum feature space is the space formed by using the three parameters  $\mu_O$ ,  $\theta_O$ , and  $\psi_O$  of the  $V_O$  operator to create a point in the unit 2-sphere. Specifically,

$$x = \mu_O \sin(\theta_O) \cos(\psi_O) \quad (25)$$

$$y = \mu_O \sin(\theta_O) \sin(\psi_O) \quad (26)$$

$$z = \mu_O \cos(\theta_O) \quad (27)$$

We first simulated qubit dynamics subject to realisations of the above noise processes with the approximated ideal CPMG pulses. We then simulated a  $1/f$  noise process with a bump in the PSD, changing the location of its peak compared to earlier noise processes, which acted as an unknown noise process.

While simulating a qubit in the presence of the realisation of an unknown noise process, we used more realistic CPMG pulses; the pulse width was increased, and the jitter was added to the peak's timing and value. From the realistic CPMG pulses, we ended up with a cluster of points in feature space arising from distinct realisations of the jitter.

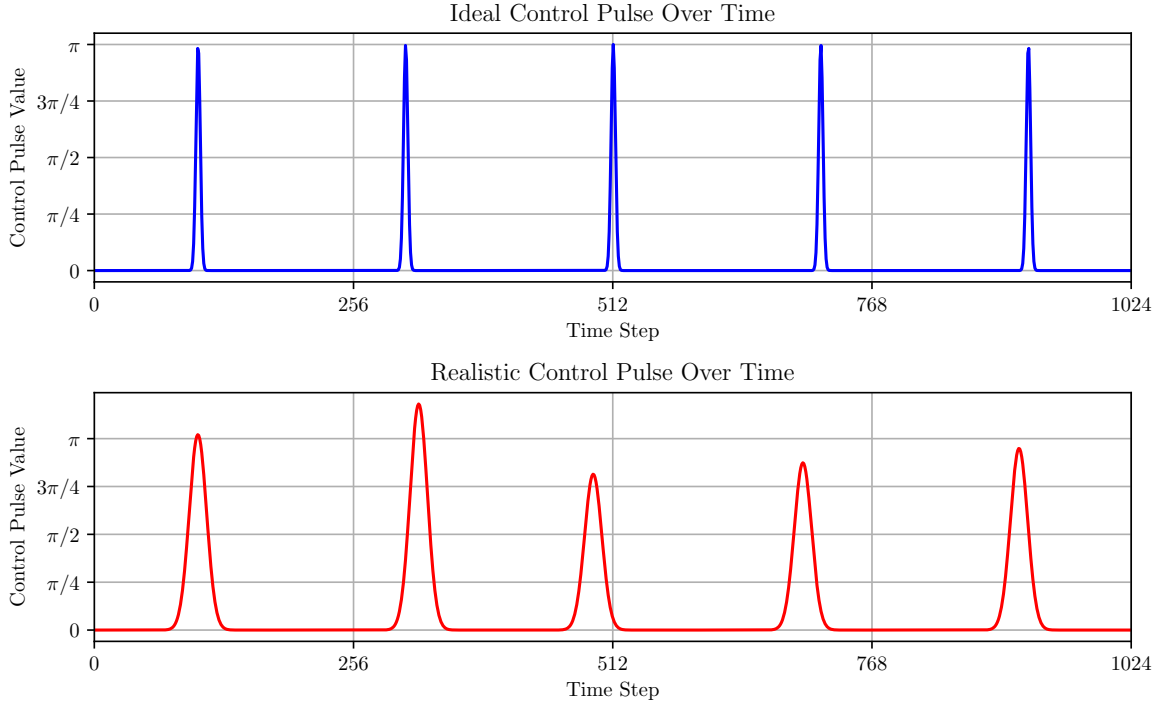


**Figure 2.** Control pulses used in the simulations. The top row shows the ideal CPMG pulses and the bottom row shows the realistic CPMG pulses.

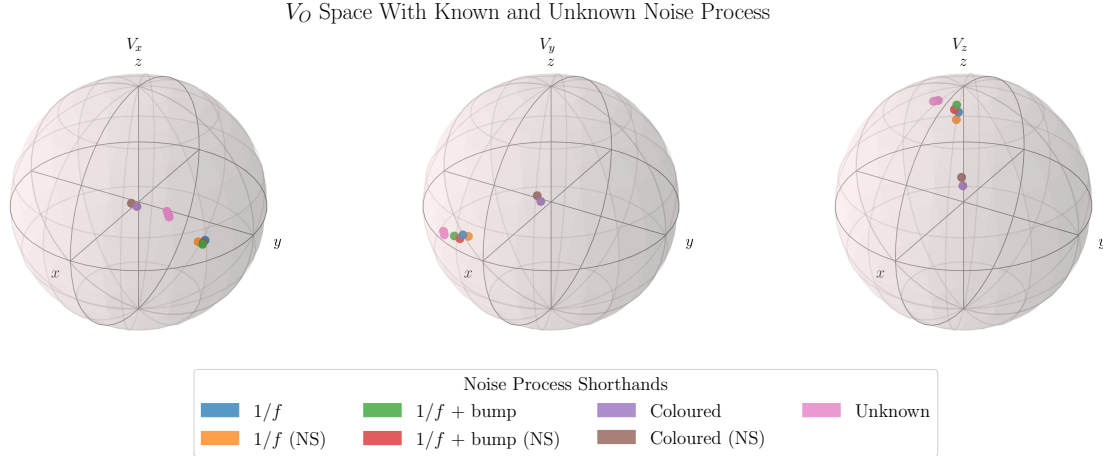
In a black box manner, we identify which noise process was present in this unknown noise process by measuring which *a priori* noise process the cluster of points was closest to in the quantum feature space.

To simulate ideal CPMG pulses, we set  $\lambda = \frac{1}{96}$ ,  $\delta_\tau = 0$ ,  $n_{\max} = 5$ , and  $A_n = \pi$ . These values were chosen to approximate delta function pulses (See Fig. 2 top row).

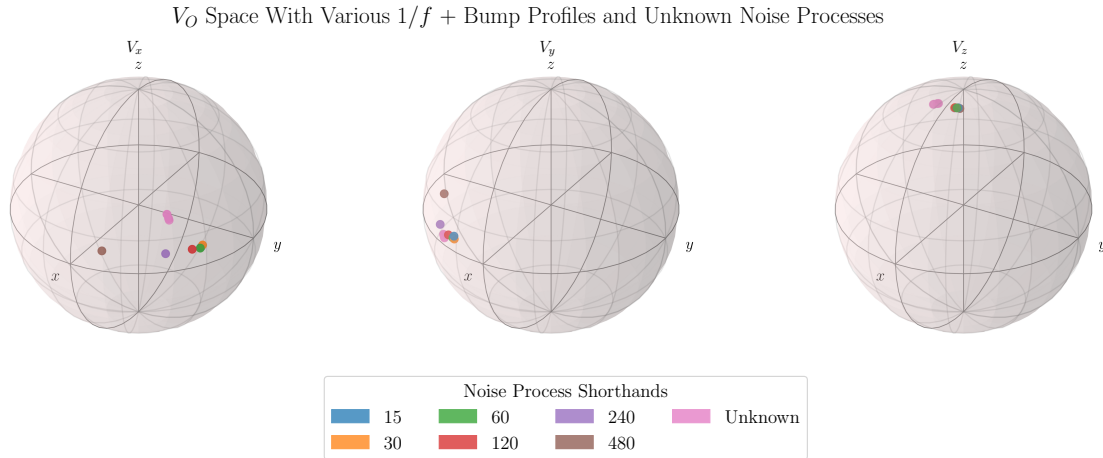
To simulate the realistic CPMG pulses we set  $\lambda = \frac{1}{24}$ ,  $\delta_\tau$  was chosen from a uniform random distribution spanning the interval  $[-\frac{24T}{M}, \frac{24T}{M}]$ , and  $A_n = \pi + \epsilon$  where  $\epsilon$  was drawn from a uniform random distribution spanning the interval  $[-\frac{\pi}{5}, \frac{\pi}{5}]$  (See Fig. 2 bottom row). Five control pulse sequences were generated with ensemble averaging over 2000 noise process realisations, resulting in a cluster of five points in the quantum feature space.

Fig. 3 presents quantum feature space visualisations on the unit 2-sphere across various noise processes utilising ideal CPMG sequences alongside the unknown noise process.

From the first round of simulations, we calculated the average of the Euclidean distances between the realistic data points and single data point for the *a priori* noise processes for the feature spaces associated with  $V_x$ ,  $V_y$ , and  $V_z$ . We found that the '1/f + bump' noise process had the smallest average Euclidean distance across all feature spaces, indicating the unknown noise process is likely closest to this noise process.



**Figure 3.** Visualisation of  $V_O$  parameter space across various noise profiles using ideal CPMG sequences and “real” data simulated with broader Gaussian pulses and additional jitter in pulse positions and amplitudes. The “real” data clusters closest to the  $1/f$  noise process with a bump in the PSD.



**Figure 4.** Visualisation of  $V_O$  parameter space across various ‘ $1/f$  + bump’ noise processes with varying peak locations in the PSD on the Gaussian bump. The unknown noise process is most similar to the  $1/f$  noise process with peaks at dimensionless frequencies 240 and 120.

To refine our understanding of the unknown noise process, we simulated several ‘ $1/f$  + bump’ noise profiles with varying peak locations in the PSD. The results indicated that the noise processes with peaks at dimensionless frequencies 240 and 120 were the closest matches, as measured by the Euclidean distance in the quantum feature space, to the unknown process, which peaks at 200.

This approach demonstrates that one could simulate a broad class of noise processes to identify the closest match to the experimental data arising from an unknown noise process. Once the general noise process is found, a binary search could be performed to estimate specific parameters of this unknown noise process.

### 5.2. Decision Tree for Noise Characterisation

We then explored the ability of ML algorithms to use this quantum feature space. To do this, we generated 600 different noise processes and trained a decision tree with K-Fold cross-validation [28, 29].

For the 600 distinct noise processes, 200 processes were  $1/f$  based, 200 were  $1/f$  with a bump based, and 200 were coloured noise based. For each noise process class, half were stationarity, and half were non-stationary, i.e. 100  $1/f$  stationary noise processes and 100  $1/f$  non-stationary noise processes. We randomised several parameters between each noise profile technique to create distinct processes to ensure a diverse and representative dataset. Table 1 summarises the randomised parameters for each noise process and the range of values used. For the  $1/f$  noise processes, the exponent ( $\alpha$ ) was varied, and for the  $1/f$  noise profiles with a bump, the bump location in the frequency domain ( $\mu$ ) was varied alongside  $\alpha$ . For coloured noise, the division factor controlling the filter was randomised. For all non-stationary profiles, the peak position as a fraction of the total time was randomised.

Noise Profile Type	Parameter	Range/Value
$1/f$ Noise Profiles	$\alpha$	[0.7, 1.3]
$1/f$ Noise Profiles with Bump	$\mu$	[0, 256]
	$\alpha$	[0.7, 1.3]
Coloured Noise	Division Factor	[2, 16]
Non-Stationary Profiles	Peak of deterministic signal	[0.1t, 0.9t]

**Table 1.** Summary of noise profile characteristics.

To analyse the noise profiles, we used a decision tree classifier from the *scikit-learn* library [29]. The decision tree classifier was trained on the combined vector components across all three quantum feature spaces, employing a 10-fold cross-validation approach. Each sample was labelled for stationarity and noise type, where two different trees were trained for each classification task. The decision tree classifier for stationarity achieved an average test accuracy of 0.90, and the noise type classifier achieved an average test accuracy of 0.95.

The feature importances for stationarity and noise type classification are shown in Table 2 and Table 3. The feature importance is calculated as the sum of the reduction in the Gini impurity index across all nodes in the tree that use the feature [29]. Interestingly, for both classification tasks, only 3-4 features are needed to explain the majority of the variance in the data, where at least one feature per observable has high importance. This demonstrates how noise process characteristics manifest themselves in the quantum feature space, which may assist in future work to clarify the mapping between a given noise process characteristic and the quantum feature space.

The high accuracy of the decision tree classifier in both tasks demonstrates the

Feature	$V_x(x)$	$V_x(y)$	$V_x(z)$	$V_y(x)$	$V_y(y)$	$V_y(z)$	$V_z(x)$	$V_z(y)$	$V_z(z)$
Importance	0.08	0.07	0.26	0.04	0.16	0.04	0.12	0.02	0.21

**Table 2.** Feature importances for classification of stationarity.

Feature	$V_x(x)$	$V_x(y)$	$V_x(z)$	$V_y(x)$	$V_y(y)$	$V_y(z)$	$V_z(x)$	$V_z(y)$	$V_z(z)$
Importance	0.03	0.28	0.16	0.15	0.01	0.01	0.00	0.01	0.35

**Table 3.** Feature importances for classification of noise type.

effectiveness of the quantum feature space parameters in distinguishing between different noise processes and determining their stationarity. These results further validate our approach and provide a robust method for characterising and classifying noise in quantum systems.

### 5.3. Properties of the $V_O$ Parameter Space

We sought to understand the mapping between control and noise parameters and the quantum feature space. For these experiments, we explored the impact of widening control pulse widths, which simulated less ideal delta function pulses, the interpolation between noise profiles, and the impact of increasing noise energy.

In Fig. 5(a), the impact within feature space of widening control pulse widths is illustrated. The visual transition in the feature space is smooth, supporting the quantum feature space as robust and showing interpolation between data points, a highly desirable characteristic of feature spaces.

The results in Fig. 5(b) are similar and show a smooth interpolation between the  $1/f$  noise process with a bump and the coloured Gaussian noise process. These interpolations were achieved by creating a linear combination of the noise processes at different ratios, progressively transitioning from one to the other.

We then investigated the impact of increasing the signal energy of the  $1/f$  with a bump and coloured Gaussian noise processes. Signal energy here is defined as,

$$E = \sum_{i=1}^N |n_i|^2 \quad (28)$$

where  $n_i$  is the noise process value at time step  $i$  and  $N$  is the total number of time steps. To implement increasing energy, we scaled all values of a given noise realisation (i.e. all  $n_i$ ) by a constant factor. Using the following scale factors: 0.5, 0.75, 1.0, 1.25, and 1.5.

As depicted in Fig. 5(c), where increasing colour saturation represents increasing energy, the trajectory in the  $V_X$  parameter space illustrates how increasing the energy of the noise drives the points further away from the identity in  $V_X$  space for both the  $1/f$

and coloured Gaussian noise processes, interestingly, this trend is not mirrored the  $V_Y$  feature space; data points move towards the identity as the energy increases. The  $V_Z$  feature space shows that points move downwards as the energy increases. These trends highlight the continuous interpolation between data points in the quantum feature space. Another notable trend is that for  $1/f$  noise, for both  $V_X$  and  $V_Y$  feature spaces, a change in the signal energy is represented by a rotation around the  $z$  axis, whereas for coloured Gaussian noise, a change results in points moving along a straight line sitting on the  $x$ - $y$  plane.

## 6. Conclusion and Future Work

This work has introduced a quantum feature space based on the  $V_O$  noise operator formalism. To create this quantum feature space, we extended the noise operator formalism to map experimental measurements directly to system-bath interaction operators. We visualised the quantum feature space, mapping its behaviour to control pulses and noise process parameters and optimising control pulses using differential evolution.

It was found that quantum feature spaces can be illuminating and can be used to identify unknown qubit noise processes without making restrictive assumptions. This feature space is a promising tool for future noise characterisation.

Future work could further refine control techniques within the quantum feature space, enhancing the ability to mitigate noise effects. In particular, exploring different types of control pulses and their parameters could provide deeper insights into optimising qubit control for various noise environments. Future work could include studying a broader range of noise processes to further validate the developed methodologies' robustness. Incorporating non-stationary and non-Gaussian noise models further helps us understand the quantum feature space. The methods developed could also be applied to systems with more qubits in both simulated and experimental settings.

## 7. Data and Code Availability

The data and code are available here:

### Acknowledgments

Matt Woolley acknowledges support from the Australian Research Council (ARC) Centre of Excellence for Engineered Quantum Systems CE170100009. Akram Youssry acknowledges support from the Australian Research Council (ARC) Discovery Project DP210101198.

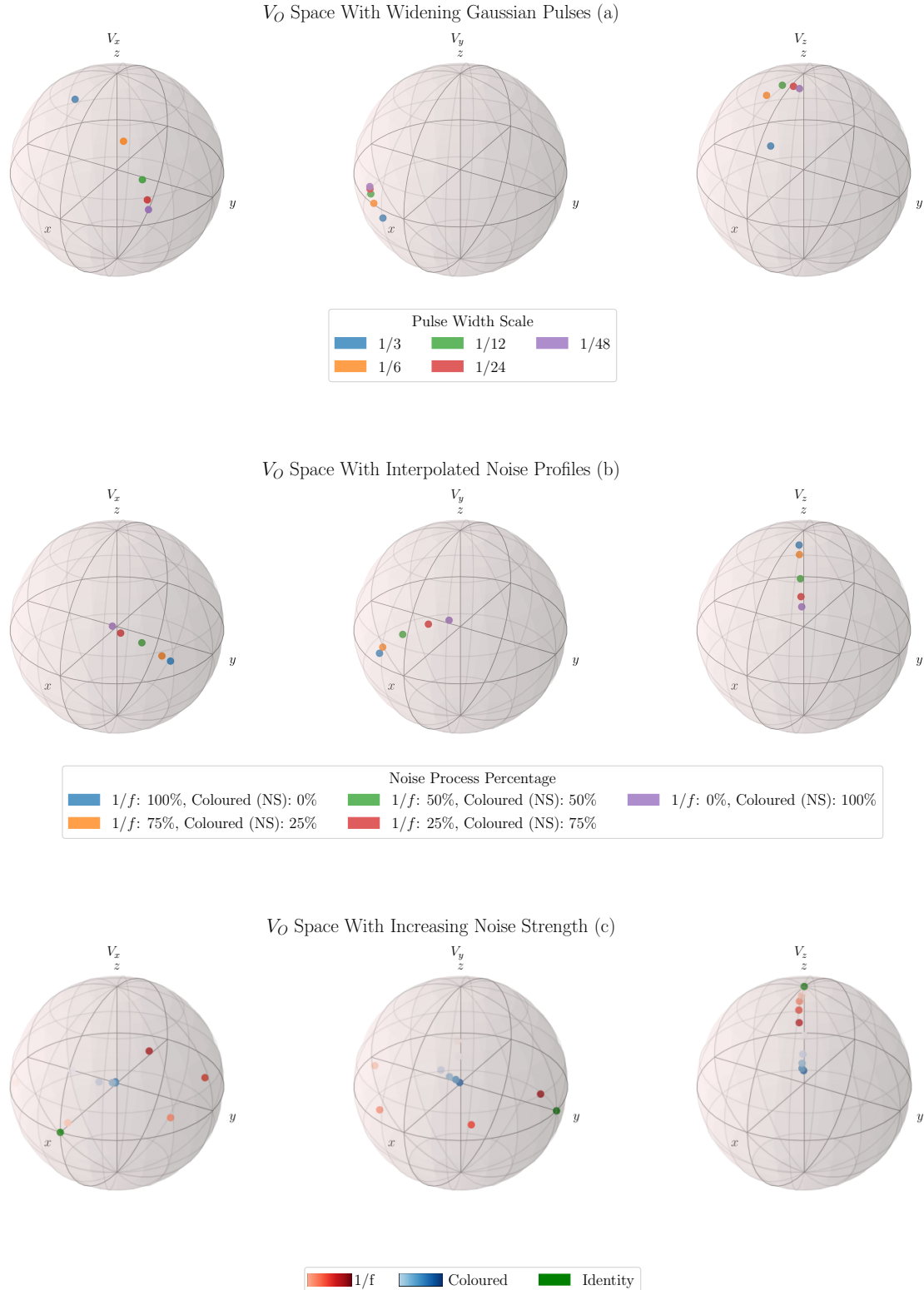


**Figure 5.** (a) Visualisation of the quantum feature space with widening Gaussian-shaped control pulses, with fraction indicating the scale factor. (b) Visualisation of the quantum feature space with interpolation between noise processes implemented by utilising a linear combination of the  $1/f$  noise process with a bump and coloured Gaussian noise process. (c) Visualisation of the quantum parameter space with two different noise processes,  $1/f$  noise process with a bump and coloured Gaussian noise process, with colour saturation representing increasing energy.

**ORCID iD**

Akram Youssry <https://orcid.org/0000-0001-7301-5834>

**8. References**

- [1] Akram Youssry, Gerardo A Paz-Silva, and Christopher Ferrie. Characterization and control of open quantum systems beyond quantum noise spectroscopy. *npj Quantum Information*, 6(1):95, 2020.
- [2] Elija Perrier, Akram Youssry, and Chris Ferrie. Qdataset, quantum datasets for machine learning. *Scientific Data*, 9(1):582, 2022.
- [3] John Preskill. Quantum computing in the nisq era and beyond. *Quantum*, 2:79, 2018.
- [4] Sergey Bravyi, Matthias Englbrecht, Robert König, and Nolan Peard. Correcting coherent errors with surface codes. *npj Quantum Information*, 4(1):1–6, 2018.
- [5] Lorenza Viola, Emanuel Knill, and Seth Lloyd. Dynamical decoupling of open quantum systems. *Physical Review Letters*, 82(12):2417, 1999.
- [6] Akram Youssry and Hendra I Nurdin. Multi-axis control of a qubit in the presence of unknown non-markovian quantum noise. *Quantum Science and Technology*, 8(1):015018, 2022.
- [7] David F Wise, John JL Morton, and Siddharth Dhomkar. Using deep learning to understand and mitigate the qubit noise environment. *PRX Quantum*, 2(1):010316, 2021.
- [8] Arian Vezvaei, Nanako Shitara, Shuo Sun, and Andrés Montoya-Castillo. Noise spectroscopy without dynamical decoupling pulses. *arXiv preprint arXiv:2210.00386*, 2022.
- [9] Stefano Martina, Santiago Hernández-Gómez, Stefano Gherardini, Filippo Caruso, and Nicole Fabbri. Deep learning enhanced noise spectroscopy of a spin qubit environment. *arXiv preprint arXiv:2301.05079*, 2023.
- [10] Sandeep Mavadia, Virginia Frey, Jarrah Sastrawan, Stephen Dona, and Michael J Biercuk. Prediction and real-time compensation of qubit decoherence via machine learning. *Nature communications*, 8(1):14106, 2017.
- [11] Riddhi Swaroop Gupta and Michael J Biercuk. Machine learning for predictive estimation of qubit dynamics subject to dephasing. *Physical Review Applied*, 9(6):064042, 2018.
- [12] Christian L Degen, Friedemann Reinhard, and Paola Cappellaro. Quantum sensing. *Reviews of modern physics*, 89(3):035002, 2017.
- [13] Jens M Boss, Kevin Chang, Julien Armijo, Kristian Cujia, Tobias Rosskopf, Jerónimo R Maze, and Christian L Degen. One-and two-dimensional nuclear magnetic resonance spectroscopy with a diamond quantum sensor. *Physical review letters*, 116(19):197601, 2016.
- [14] Herman Y Carr and Edward M Purcell. Effects of diffusion on free precession in nuclear magnetic resonance experiments. *Physical review*, 94(3):630, 1954.
- [15] Saul Meiboom and David Gill. Modified spin-echo method for measuring nuclear relaxation times. *Review of scientific instruments*, 29(8):688–691, 1958.
- [16] Gonzalo A Álvarez and Dieter Suter. Measuring the spectrum of colored noise by dynamical decoupling. *Physical review letters*, 107(23):230501, 2011.
- [17] Uwe von Lüpke, Félix Beaudoin, Leigh M Norris, Youngkyu Sung, Roni Winik, Jack Y Qiu, Morten Kjaergaard, David Kim, Jonilyn Yoder, Simon Gustavsson, et al. Two-qubit spectroscopy of spatiotemporally correlated quantum noise in superconducting qubits. *PRX Quantum*, 1(1):010305, 2020.
- [18] Won Kyu Calvin Sun and Paola Cappellaro. Self-consistent noise characterization of quantum devices. *Physical Review B*, 106(15):155413, 2022.
- [19] Stefano Martina, Stefano Gherardini, and Filippo Caruso. Machine learning approach for quantum non-markovian noise classification. *arXiv preprint arXiv:2101.03221*, 2021.
- [20] Alessandro Baroni, Joseph Carlson, Rajan Gupta, Andy CY Li, Gabriel N Perdue, and Alessandro

- Roggero. Nuclear two point correlation functions on a quantum computer. *Physical Review D*, 105(7):074503, 2022.
- [21] Amanda E Seedhouse, Nard Dumoulin Stuyck, Santiago Serrano, Tuomo Tanttu, Will Gilbert, Jonathan Yue Huang, Fay E Hudson, Kohei M Itoh, Arne Laucht, Wee Han Lim, et al. Spatio-temporal correlations of noise in mos spin qubits. *arXiv preprint arXiv:2309.12542*, 2023.
- [22] Kiyoto Nakamura and Joachim Ankerhold. Gate operations for superconducting qubits and non-markovianity: Fidelities, long-range time correlations, and suppression of decoherence. *arXiv preprint arXiv:2402.18518*, 2024.
- [23] Youngkyu Sung, Félix Beaudoin, Leigh M Norris, Fei Yan, David K Kim, Jack Y Qiu, Uwe von Lüpke, Jonilyn L Yoder, Terry P Orlando, Simon Gustavsson, et al. Non-gaussian noise spectroscopy with a superconducting qubit sensor. *Nature communications*, 10(1):3715, 2019.
- [24] Michael A Nielsen and Isaac Chuang. Quantum computation and quantum information, 2002.
- [25] Roger Penrose. A generalized inverse for matrices. In *Mathematical proceedings of the Cambridge philosophical society*, volume 51, pages 406–413. Cambridge University Press, 1955.
- [26] Adam Paszke, Sam Gross, Francisco Massa, Adam Lerer, James Bradbury, Gregory Chanan, Trevor Killeen, Zeming Lin, Natalia Gimelshein, Luca Antiga, et al. Pytorch: An imperative style, high-performance deep learning library. *Advances in neural information processing systems*, 32, 2019.
- [27] Charles R. Harris, K. Jarrod Millman, Stéfan J. van der Walt, Ralf Gommers, Pauli Virtanen, David Cournapeau, Eric Wieser, Julian Taylor, Sebastian Berg, Nathaniel J. Smith, Robert Kern, Matti Picus, Stephan Hoyer, Marten H. van Kerkwijk, Matthew Brett, Allan Haldane, Jaime Fernández del Río, Mark Wiebe, Pearu Peterson, Pierre Gérard-Marchant, Kevin Sheppard, Tyler Reddy, Warren Weckesser, Hameer Abbasi, Christoph Gohlke, and Travis E. Oliphant. Array programming with NumPy. *Nature*, 585(7825):357–362, September 2020.
- [28] Gareth James. An introduction to statistical learning, 2013.
- [29] F. Pedregosa, G. Varoquaux, A. Gramfort, V. Michel, B. Thirion, O. Grisel, M. Blondel, P. Prettenhofer, R. Weiss, V. Dubourg, J. Vanderplas, A. Passos, D. Cournapeau, M. Brucher, M. Perrot, and E. Duchesnay. Scikit-learn: Machine learning in Python. *Journal of Machine Learning Research*, 12:2825–2830, 2011.